Biochimie 91 (2009) 596–603

Contents lists available at ScienceDirect

Biochimie

journal homepage: www.elsevier.com/locate/biochi

Research paper

Peculiar inhibition of human mitochondrial aspartyl-tRNA synthetase by adenylate analogs

Marie Messmer [a], Sébastien P. Blais [b], Christian Balg [c], Robert Chênevert [c], Luc Grenier [b], Patrick Lagüe [b], Claude Sauter [a], Marie Sissler [a], Richard Giegé [a], Jacques Lapointe [b], Catherine Florentz [a,*]

[a] Architecture et Réactivité de l'ARN, Université Louis Pasteur, CNRS, IBMC 15 rue René Descartes, 67084 Strasbourg Cedex, France
[b] Département de Biochimie et de Microbiologie, Centre de recherche sur la fonction, la structure et l'ingénierie des protéines (CREFSIP), Faculté des sciences et de génie, Université Laval, Québec, Canada G1V 0A6
[c] Département de Chimie, Centre de recherche sur la fonction, la structure et l'ingénierie des protéines (CREFSIP), Faculté des sciences et de génie, Université Laval, Québec, Canada G1V 0A6

ARTICLE INFO

Article history:
Received 16 December 2008
Accepted 18 February 2009
Available online 28 February 2009

Keywords:
Human mitochondria
Aspartyl-tRNA synthetase
Inhibition
Adenylate analogs
Molecular docking

ABSTRACT

Human mitochondrial aminoacyl-tRNA synthetases (mt-aaRSs), the enzymes which esterify tRNAs with the cognate specific amino acid, form mainly a different set of proteins than those involved in the cytosolic translation machinery. Many of the mt-aaRSs are of bacterial-type in regard of sequence and modular structural organization. However, the few enzymes investigated so far do have peculiar biochemical and enzymological properties such as decreased solubility, decreased specific activity and enlarged spectra of substrate tRNAs (of same specificity but from various organisms and kingdoms), as compared to bacterial aaRSs. Here the sensitivity of human mitochondrial aspartyl-tRNA synthetase (AspRS) to small substrate analogs (non-hydrolysable adenylates) known as inhibitors of *Escherichia coli* and *Pseudomonas aeruginosa* AspRSs is evaluated and compared to the sensitivity of eukaryal cytosolic human and bovine AspRSs. L-aspartol-adenylate (aspartol-AMP) is a competitive inhibitor of aspartylation by mitochondrial as well as cytosolic mammalian AspRSs, with K_i values in the micromolar range (4–27 μM for human mt- and mammalian cyt-AspRSs). 5′-*O*-[*N*-(L-aspartyl)sulfamoyl]adenosine (Asp-AMS) is a 500-fold stronger competitive inhibitor of the mitochondrial enzyme than aspartol-AMP (10 nM) and a 35-fold lower competitor of human and bovine cyt-AspRSs (300 nM). The higher sensitivity of human mt-AspRS for both inhibitors as compared to either bacterial or mammalian cytosolic enzymes, is not correlated with clear-cut structural features in the catalytic site as deduced from docking experiments, but may result from dynamic events. In the scope of new antibacterial strategies directed against aaRSs, possible side effects of such drugs on the mitochondrial human aaRSs should thus be considered.

1. Introduction

Two distinct translational machineries coexist in mammalian cells. The mitochondrial machinery is still in the process of characterization. While its 22 tRNAs, 11 mRNAs (2 are polycistronic) that code for 13 proteins, and 2 rRNAs are encoded by the mitochondrial (mt) genome, all other macromolecules needed for protein synthesis are coded by the nuclear chromosome, synthesized within the cytosol and imported [1]. They include the sets of aminoacyl-tRNA synthetases (aaRSs), ribosomal proteins, translation factors and tRNA maturation and modification enzymes. AaRSs are the enzymes which catalyze specific esterification of their cognate tRNAs by the corresponding amino acids. Most of the genes encoding the human aaRSs have been annotated, demonstrating their distribution into two distinct sets [2,3]. Except for GlyRS [4,5] and LysRS [6], mt- and cytosolic-aaRSs (cyt-aaRSs) are encoded by distinct genes.

In agreement with the endosymbiotic hypothesis for the origin of mitochondria [7,8], sequence features and modular organization of many mt-aaRSs are of bacterial-type and thus differ from the eukaryotic-type corresponding cyt-aaRSs [9]. Biochemical and enzymatic characterization of an initial set of human bacterial-type mt-aaRSs revealed however unexpected properties making these enzymes functionally distinct from their bacterial counterparts. As

Abbreviations: aaRS, aminoacyl-tRNA synthetase, with aa for the amino acid in three-letter abbreviation; mt, mitochondrial; cyt, cytosolic; aspartol-AMP, aspartol-adenylate; Asp-AMS, 5′-*O*-[*N*-(L-aspartyl)sulfamoyl]adenosine.

* Corresponding author. Tel.: +33 3 88 41 70 59; fax: +33 3 88 60 22 18.
E-mail address: c.florentz@ibmc.u-strasbg.fr (C. Florentz).

0300-9084/$ – see front matter © 2009 Elsevier Masson SAS. All rights reserved.
doi:10.1016/j.biochi.2009.02.005

an example, human mt-AspRS and mt-TyrRS share about 40% sequence identity with the corresponding *Escherichia coli* enzymes (including strongly conserved functional amino acids) and present the same modular organization [2]. The crystallographic structure of mt-TyrRS reveals a three-dimensional fold very similar to that of *Bacillus subtilis* and *E. coli* TyrRSs [10]. However, both mt-aaRSs aminoacylate their substrates with 10- to 40-fold less efficiency than the corresponding *E. coli* aaRSs [2]. These mt-enzymes require restricted sets of identity elements within their cognate tRNAs compared to bacterial AspRSs [11] or TyrRSs [12]. Finally, both mt-AspRS and mt-TyrRS likely have an enlarged spectrum of possible tRNA substrates, as first observed after comparing *E. coli* aaRSs with homologous bovine enzymes [13]. Indeed mitochondrial enzymes aminoacylate tRNAs of same specificity from a large range of organisms, while most bacterial enzymes recognize and aminoacylate only their own tRNA.

Aminoacyl-tRNA synthetases have been subjected to significant evolutionary divergence, so that selective inhibition of bacterial enzymes appears as a valuable strategy for the production of new antibiotics (reviewed in Refs. [14–18]). Such antibiotics are expected to have strong negative effects on pathogenic bacteria, but should not affect the human host. Pseudomonic acid (mupirocin) is the first known effective antibiotic of this type and inhibits IleRSs from Gram positive (e.g. *Staphylococcus aureus*) and Gram negative (e.g. *Neisseria meningitidis*) bacteria with a 8000-fold higher affinity than for mammalian cyt-IleRS [19,20]. This natural product is a stable adenylate analog and is in clinical use [21]. Beside IleRS, many other aaRSs are inhibited by adenylate derivatives, of synthetic and in a few cases of natural origin, that can be considered as potential drugs targeting aaRSs [14–17].

We have previously synthesized aspartyl-adenylate analogs [22], and established that they have inhibitory effects on bacterial aaRSs as tested on *E. coli* and *Pseudomonas aeruginosa* AspRSs [22]. Here, the effect of Asp-AMS and aspartol-AMP (Fig. 1) is explored on human mt-AspRS as well as on mammalian cytosolic AspRSs (human and bovine). The inhibition produced by Asp-AMS and aspartol-AMP on the activity of the three enzymes was investigated and compared with the effect produced on bacterial AspRSs. Functional studies were completed by computer-assisted docking of the adenylates in the catalytic site of the diverse AspRSs. Data reveal differences between the three types of enzymes (bacterial, mt- and cyt-eukaryal) and strikingly highest sensitivity of the mitochondrial enzyme to both inhibitors. They further support functional differences between the bacterial-type human mt-AspRS and bacterial AspRSs. These functional peculiarities are not due to striking structural idiosyncrasies in the catalytic domain of the AspRSs, in particular of human mt-AspRS, as suggested by docking of the adenylate in the catalytic sites. Structure–function relationships and the implications for medical research dedicated to the discovery of new antibiotics using aaRSs as targets will be discussed.

2. Materials and methods

2.1. Materials and enzymes

Total *E. coli* tRNA was purchased from Roche Diagnostics and total calf liver tRNA from Novagen. L-[2,3-^{3}H]aspartic acid (specific activity 34 Ci/mmol) was from GE Healthcare. Aspartol-AMP and Asp-AMS were synthesized as reported [22]. Ni-NTA resin was from Qiagen Inc. Human (*Homo sapiens*) mt-AspRS was previously cloned into pQE70 vector that introduces a poly-His tag to the C-terminus of the expressed protein. Overproduction and purification steps were conducted as described [2]. Human cyt-AspRS was a kind gift of M. Frugier (Stasbourg). Bovine *(Bos taurus)* cyt-AspRS was purchased from Bio S&T Inc. (Montreal, Canada) as a mixture of different aminoacyl-tRNA synthetases.

2.2. Aminoacylation and inhibition assays

Aspartylation assays in the presence of human mt-AspRS were carried out in 50 mM HEPES-NaOH pH 7.5, 2.5 mM ATP, 12 mM $MgCl_2$, 25 mM KCl, 0.2 mg/ml BSA, 1 mM spermine and 40 μM total *E. coli* tRNA. For establishing the K_m for aspartate, this substrate was added at concentrations ranging from 0.7 to 40 μM. The reaction was initiated by adding the pre-warmed enzyme at 37 °C to a final concentration of 62.5 nM. The amount of aspartyl-tRNA formed was determined by the radioactivity present in 5% trichloroacetic acid precipitates of reaction mixture aliquots, as previously described [23]. Initial reaction rates were determined by measuring [^{3}H]aspartyl-tRNA formed in 5 μl aliquots (from a total volume of 50 μl) taken at 1 min intervals over 6 min. Inhibition constants (K_i) were determined at the aspartate concentration corresponding to the K_m value and the inhibitors aspartol-AMP and Asp-AMS were added at various concentrations from 0.5 to 100 μM and from 1 to 50 nM, respectively, to reaction media pre-heated to 37 °C, 2 min before addition of the synthetase. The error range was 15% for triplicate experiments.

Aspartylation assays performed in the presence of human cyt-AspRS were carried out as for human mt-AspRS but with 80 μM total calf tRNA and 0.5 nM enzyme. To determine the K_m for aspartate for the human cyt-AspRS, this substrate was added to final concentrations ranking from 2.5 to 120 μM. Aliquots of 5 μl were taken from a total volume of 50 μl, at 2 min intervals over 12 min and treated as described above. Establishment of K_i for aspartol-AMP and Asp-AMS was set to 24 μM of aspartate (K_m value) and was done as described above but with inhibitor concentrations varying from 5 μM to 100 μM and from 50 nM to 1 μM, respectively. The error range was 10% for triplicate experiments.

2.3. Determination of inhibition type and constant (K_i)

The K_m values of human cyt-AspRS and human mt-AspRS for the aspartate substrate were calculated from Michaelis–Menten plots.

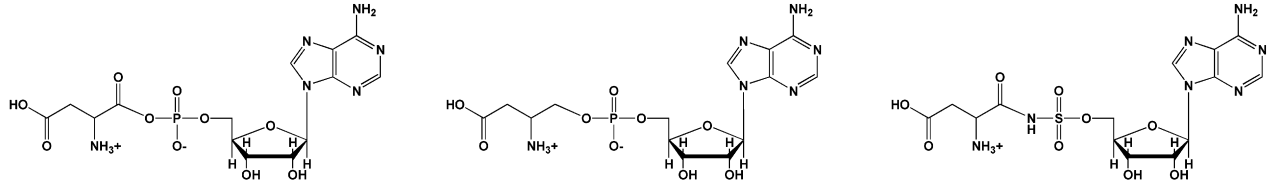

Fig. 1. Comparison of the chemical structures of aspartyl-adenylate and its two analogs, L-aspartol-adenylate and 5′-*O*-[*N*-(L-aspartyl)sulfamoyl]adenosine.

The rate 'v_i' of the aminoacylation reaction in the presence of inhibitor at various concentrations [I] is given by the following equation:

$$v_i = \frac{V_{max}[S]}{[S] + K_m(1 + ([I]/K_i))} \quad (1)$$

When reactions are conducted at the amino acid concentration corresponding to the K_m value and in the presence of saturating concentrations of ATP and tRNA, Eq. (1) can be rearranged as Eq. (2), with the ratio v_i/v_0 (where v_0 is the rate in the absence of inhibitor under the same substrate concentrations) expressed as a function of [I]. This equation illustrates competitive inhibition with one binding site for the inhibitor [24], and can be simplified in Eq. (3) when $[S] = K_m$:

$$\frac{v_i}{v_0} = \frac{[S] + K_m}{[S] + K_m(1 + ([I]/K_i))} \quad (2)$$

$$\frac{v_i}{v_0} = \frac{2}{2 + ([I]/K_i)} \quad (3)$$

Curve-fitting of the data was made with the Sigmaplot software (SPSS Inc) and was used to identify the type of inhibition and to calculate the K_i values. Inhibition type of Asp-AMS with respect to aspartate for both human AspRSs was further confirmed by the determination of the apparent K_m for aspartate in the presence of several concentrations of this inhibitor (from 0 to 40 nM for human mt-AspRS and from 0 to 1.2 μM for human cyt-AspRS) and under fixed and saturating concentrations of the two other substrates (2.5 mM ATP and 40 μM *E. coli* total tRNA for human mt-AspRS or 80 μM total calf tRNA for human cyt-AspRS).

2.4. Docking of adenylate and analogs

Three-dimensional models of candidate AspRSs were derived from crystallographic structures of close relatives in complex with tRNA. Yeast binary complex (1ASY.pdb – Ref. [25]) and the *E. coli* ternary complex (1CA0.pdb – Ref. [26]) were used to model bovine and human cyt-AspRSs and bacterial-type enzymes (*P. aeruginosa* and human mitochondria, respectively). The three-dimensional model of the mt-AspRS was built using modeler [27] as described previously [11], whereas others were generated using the web-based SWISS-MODEL workspace [28].

Docking of the natural aspartyl-adenylate and of two analogs (Asp-AMS and aspartol-AMP) was performed using AUTODOCK 3.0.5 [29]. Hydrogen atoms were added to proteins and ligands using AutoDockTools (http://www.python.org/about/website/). Gast-Eigen charges were computed for the ligand partial atomic charges.

Three-dimensional grids of interaction energies based on the macromolecular target using the AMBER force field were calculated using AutoGrid. The cubic grid box of 60 Å size (x, y, z) with a spacing of 0.375 Å and grid maps were centered on the respective AspRS active sites. Automated docking studies were carried out to evaluate the binding free energy of the inhibitors within the macromolecules. The GA-LS search algorithm (algorithm with local search) was chosen to search for the best conformers. The parameters were set using the software ADT. For all docking parameters, default values were used with 30 independent docking runs for each docking case. Each three-dimensional model was used as a rigid scaffold, but the three ligands benefited from a full freedom with respect to their flexibility to be able to adapt to the catalytic groove. A theoretical K_i value was derived from the calculated binding free energy [$K_i = \exp(\Delta G_{binding}/RT)$]. An average p$K_i$ value (p$K_i = -\log K_i$) is given for all trials falling within 2 Å rmsd from the position of the natural adenylate in crystallographic structure of *E. coli* ternary complex. The figure presenting docking results was prepared with PyMOL (DeLano Scientific LLC, CA).

3. Results

3.1. Activity of human and bovine AspRSs inhibited by aspartyl-adenylate analogs

As a prerequisite to the search of the inhibition of adenylates on AspRS activity [24] (see Materials and methods) we determined the K_m for aspartate of human cyt- and mt-AspRSs and for bovine cyt-AspRS. Initial rates of aspartylation, established under saturating tRNA and ATP concentrations were obtained for aspartate concentrations ranging from 1 to 40 μM (mt-AspRS) and 2.5 to 120 μM (cyt-AspRSs) (Fig. 2, top). Analysis of the Lineweaver–Burk plots (Fig. 2, bottom) yielded similar K_m values for the two cytosolic AspRSs (24 μM and 37 μM for the human and bovine enzymes, respectively) and a strikingly lower value (1.5 μM) for the human mt-AspRS.

The inhibition constants (K_i) of Asp-AMS and aspartol-AMP have been determined with respect to aspartate for the three AspRSs at

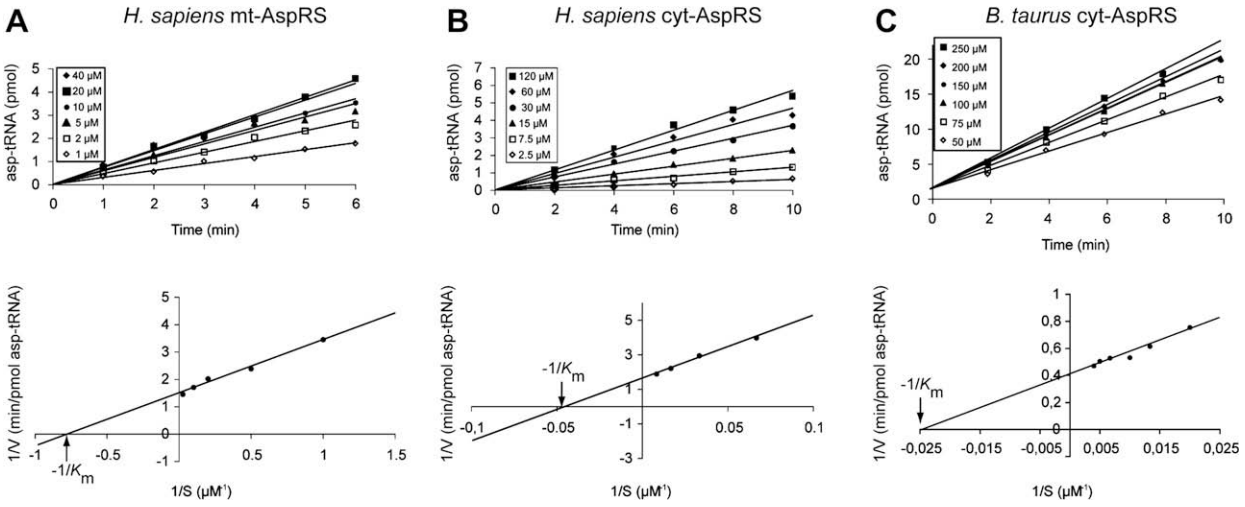

Fig. 2. Determination of the apparent K_m values for aspartate for *H. sapiens* mt-AspRS (A), *H. sapiens* cyt-AspRS (B) and for *B. taurus* cyt-AspRS (C).

fixed and saturating concentrations of ATP and tRNA and at K_m concentration for the aspartic acid. Kinetic data were displayed as normalized initial rates of tRNA aminoacylation (v_i/v_0,) as a function of inhibitor concentration I_i (with v_i being the initial rates in the presence of inhibitor and v_0 the rate in the absence of inhibitor). If inhibitions are competitive, as can be anticipated for adenylate analogs, experimental data should fit on sigmoidal curves (see Materials and methods). The theoretical sigmoidal curves computed for aspartol-AMP fit perfectly with the experimental points (Fig. 3), indicating that the inhibition is indeed competitive for the three enzymes with K_i values ranging from 4.6 to 27 μM (Table 1). In the experiments done in the presence of Asp-AMS, the fit is less perfect, especially in the case of the human mt-AspRS. Assuming inhibitions are competitive, extracted K_i values are quite similar for the two mammalian cyt-AspRSs (390 and 280 nM for the human and bovine enzymes) and 9.8 nM for the mt-AspRS. These values are 2–3 orders of magnitude below those measured for aspartol-AMP (Table 1).

To verify whether the deviations from the theoretical curve with Asp-AMS originate from experimental errors or result from a more complex kinetic behavior, we undertook a classical Lineweaver–Burk analysis for the human mitochondrial and cytosolic enzymes (Fig. 4). Apparent K_m values for aspartate have been determined under large ranges of inhibitor concentrations. All lines cross the *y*-axis into a single point that corresponds to $1/V_{max}$, conclusively demonstrating that inhibition by Asp-AMS is of competitive type with respect to aspartate both for human cyt-AspRS and mt-AspRS. Kinetic parameters in these experiments are very close to those reported in Table 1.

3.2. Molecular docking of aspartyl adenylate and analogs in the active site of AspRSs

Three-dimensional models of four AspRSs (from *P. aeruginosa*, human mitochondria, human and bovine cytoplasms) were generated to study the binding of aspartyl-adenylate and its analogs (Asp-AMS and aspartol-AMP) by molecular docking. These three-dimensional models were based on X-ray structures from *E. coli* and yeast AspRS:tRNA^{Asp} complexes (see Materials and methods). Individual monomers were considered (i.e. one active site) in the absence of tRNA. In order to get comparative scores, docking trials were performed for each ligand, both on the original X-ray structures and on the four models (with protein backbone and side chain orientation maintained as in the reference X-ray structures). The results are presented in Fig. 5. In the case of bacterial-type enzymes, the natural adenylate systematically gives a slightly better score, probably due to a structural bias: the X-ray coordinates from *E. coli* complex used as a template for homology modeling did contain this ligand. The difference of 3 theoretical pK_i units between bacterial- and eukaryotic-type systems may also be linked to the resolution of the original template, the *E. coli* structure determined with a higher accuracy (2.3 *vs* 2.9 Å resolution) giving the highest docking scores. Beside these technical aspects, the most striking feature is that pK_i values obtained for a given AspRS do not dramatically vary from one ligand to the others. Moreover, no significant behavior difference is detected between AspRSs belonging to the same group.

As an illustration, Fig. 5 shows the locations of aspartyl-adenylate, aspartol-AMP and Asp-AMS superimposed in the active site human mt-AspRS (in the homology model of *E. coli* AspRS). The docking suggests excellent superimpositions of the adenine (Fig. 5A, right) and aspartate (Fig. 5A, left) moieties at the distal extremities of the adenylate molecules and slight changes in the orientation of the ribo-phosphate and ribo-sulfamoyl groups in the central part of these molecules.

4. Discussion

4.1. General considerations

Aminoacyl-tRNA synthetases catalyze the esterification of their cognate tRNA with the specific amino acid in a two-step process. In the first step, the amino acid is recognized by the enzyme and reacts with ATP to form an enzyme-bound mixed anhydride (aa-AMP or aminoacyl-adenylate) with release of pyrophosphate [30]. In this intermediate, the high-energy anhydride bond activates the carboxyl group of the amino acid. In the second step, the activated amino acid is transferred to the 3′-terminal adenosine of the corresponding tRNA to form aminoacyl-tRNA and AMP (reviewed in Refs. [31,32]). This overall mechanism applies to both class I and class II aaRSs (reviewed in Refs. [33,34]). While the overall functioning of aaRSs is essentially conserved in evolution, one notes idiosyncrasies when comparing properties of aaRSs from phylogenetically distant species or organelles [35] and this opens the possibility to find or design species-selective inhibitors of aaRSs.

Here we focus on human mt-AspRS for a better understanding of its functional and structural idiosyncrasies, especially in regard of inhibition by small substrate analogs targeting its catalytic site. For comparative purposes, two novel mammalian cyt-AspRSs (human and bovine) were studied for their behavior to interact with aspartic acid and two adenylate analogs. Table 1 reports the K_m and K_i values for the three mammalian enzymes and compares these values with those previously determined for *E. coli* and *P. aeruginosa* AspRSs [22]. Remarkable variations are observed that are best visualized in the

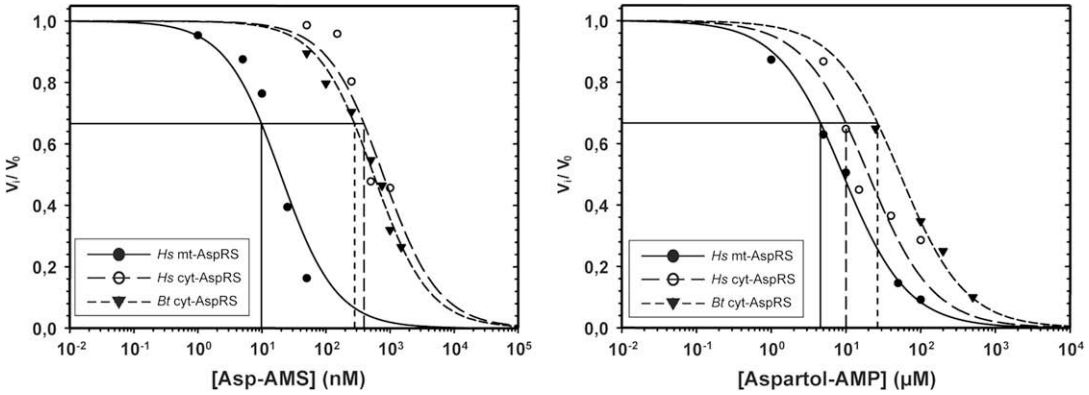

Fig. 3. Inhibition kinetics with Asp-AMS (left) and aspartol-AMP (right) of *H. sapiens* mt-AspRS, *H. sapiens* cyt-AspRS and *B. taurus* cyt-AspRS. Abbreviations used: *Hs*, *Homo sapiens*; *Bt*, *Bos taurus*.

Table 1
Kinetic parameters K_m of aspartyl-adenylate and K_i of non-hydrolysable analogs for mammalian and bacterial AspRSs. Abbreviations used: *Pa*, *Pseudomonas aeruginosa*; *Ec*, *Escherichia coli*; *Hs*, *Homo sapiens*; *Bt*, *Bos taurus*. n.d. stands for non-determined.

AspRSs	Substrates		
	Aspartate K_m (μM)	Aspartol-AMP K_i (μM)	Asp-AMS K_i (nM)
Hs mt-AspRS	1.5	4.6	9.8
Hs cyt-AspRS	24	10	390
Bt cyt-AspRS	37	27	280
Pa AspRS[a]	100	41	n.d.
Ec AspRS[a]	90	45	15

[a] Experimental data taken from Ref. [22].

histogram comparing the inverse of the K_m and K_i values (Fig. 6). Human mt-AspRS presents the most atypical functional behavior deviating significantly from what observed with other AspRSs. It is common sense to believe that the functional differences are due to structural idiosyncrasies of the different AspRSs, but as shown in other tRNA aminoacylation systems, large functional differences could originate from faint structural effects [36,37]. For interpretation of the present data it should be kept in mind that all the above results were obtained by kinetic analyses conducted in the presence of tRNA, and that former experiments with yeast AspRS have shown that $tRNA^{Asp}$ significantly increases the affinity of aspartyl-adenylate for the synthetase [38,39].

4.2. Aspartol-AMP and Asp-AMS are competitive inhibitors of H. sapiens *and* B. taurus *AspRSs*

Aspartol-AMP and Asp-AMS are analogs of aspartyl-adenylate, the natural derivative formed by AspRS in the presence of aspartic acid and ATP, during the first step of the aminoacylation reaction. Aspartol-AMP differs from aspartyl-adenylate in converting an aminoacyl-adenylate into an aminoalcohol-adenylate, while Asp-AMS has a sulfamoyl function (Fig. 1). In a previous work, it was shown as anticipated, that both molecules are competitive inhibitors of aspartate in bacterial AspRSs (*E. coli* and *P. aeruginosa*) [22,40]. While aspartol-AMP is a weak inhibitor for these two AspRSs with K_i values in the micromolar (μM) range, Asp-AMS is a strong inhibitor with K_i in the nanomolar (nM) range (Table 1). In the present work, that extends the analysis to eukaryal cyt-AspRSs (human and bovine) and to human mt-AspRS, both adenylate analogs behave also as competitive inhibitors. Inhibition constants (K_i) of aspartol-AMP remain in the μM range and those of Asp-AMS remain in the nM range, as was the case for the bacterial enzymes [22,40]. Interestingly, both cytosolic mammalian AspRSs (human and bovine) have about the same K_i for aspartol-AMP (10 and 27 μM) and for Asp-AMS (390 and 280 nM). Over the 5 enzymes considered, human mt-AspRS is the most sensitive enzyme towards each inhibitor with a K_i of 4.6 μM for aspartol-AMP and of 9.8 nM for Asp-AMS (Table 1).

4.3. H. sapiens *mitochondrial AspRS is more sensitive to adenylates than bacterial AspRSs*

The data of Table 1 and Fig. 6 highlight distinct behaviors for the three families of enzymes considered (bacterial, bacterial-type, eukaryal). Considering either K_m values for the natural substrate aspartate or K_i values of the inhibitors, the mitochondrial enzyme behaves apart from the four other AspRSs discussed here. Not only is aspartic acid retained with the best relative affinity for this enzyme (assuming that the inverse of K_m values is representative of the affinity) but also the adenylate analogs do present the highest relative inhibitory properties.

Mt-AspRS displays a much higher affinity for aspartic acid than the two cyt-AspRSs (16–25-fold) and than the two bacterial AspRSs (60–70-fold). This markedly small K_m value is in support of distinct kinetic properties for the enzyme families considered and especially of the mitochondrial bacterial-type enzyme as compared to the two other families. Bacterial synthetases (*E. coli* and *P. aeruginosa*) present the poorest affinity for their amino acid substrate, while the two eukaryal enzymes present a 3–4-fold better affinity.

In regard to inhibitors, aspartol-AMP presents a 2–6-fold lower K_i for mt-AspRS than for the human or bovine cyt-AspRSs and about 10-fold lower than the bacterial AspRSs. Asp-AMS has also the highest inhibitory effect for the mitochondrial enzyme, but it remains close to those measured for *E. coli* AspRS but distinguishes strongly from the cyt-enzymes. In summary, whatever the inhibitor, it has the strongest effect on the mitochondrial enzyme. This enzyme distinguishes thus from both other families of considered AspRSs, namely bacterial and eukaryal cytosolic AspRSs. Note that both these families present an inverted reactivity, with inhibition by aspartol-AMP more important with the eukaryal enzymes and inhibition by Asp-AMS more important with the prokaryal enzymes.

4.4. Search for structure–function relationships

Two aspects have to be considered here. First, the functional difference between the human mt-AspRS and the two bacterial AspRSs from *E. coli* and *P. aeruginosa*, given the fact that the human enzyme is of bacterial-type [2] and thus structurally similar to bacterial AspRSs. Second, the strong inhibitory effect produced by Asp-AMS with an affinity about three orders of magnitude higher than the closely related aspartol-AMP (Fig. 6). In the absence of

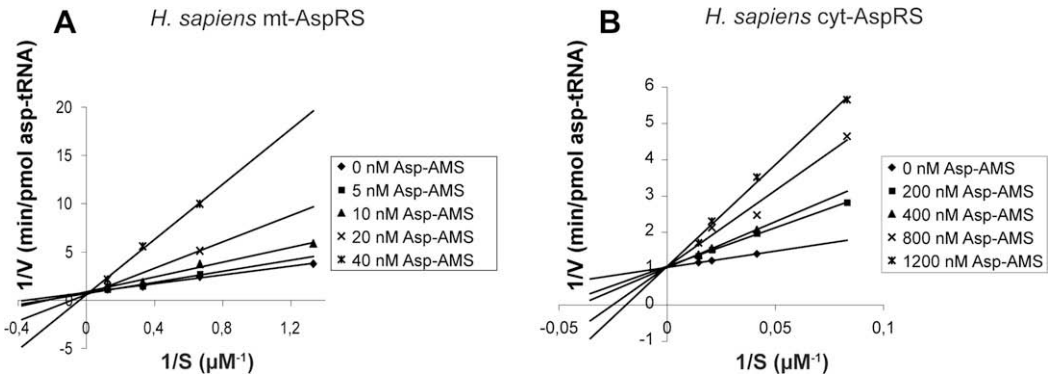

Fig. 4. Inhibition with Asp-AMP of the aminoacylation activity of *H. sapiens* mt-AspRS (A) and cyt-AspRS (B). Experiments have been performed in the presence of different fixed concentrations of Asp-AMS.

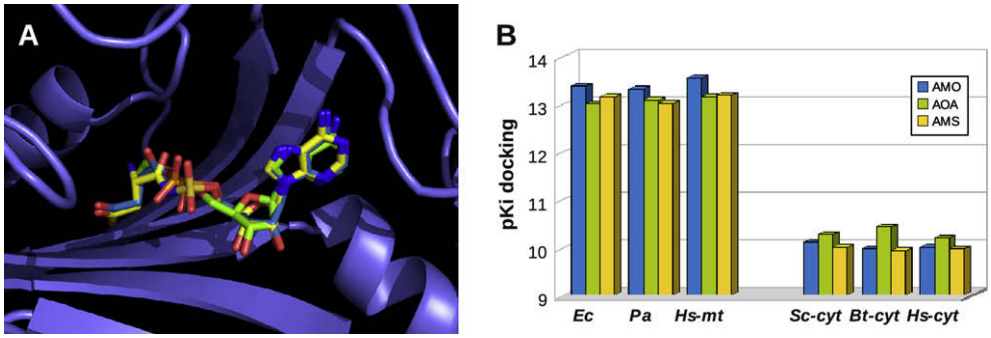

Fig. 5. Docking of aspartyl-adenylate and of two analogs in the active site of AspRSs. (A) Example of the best docking solution (i.e. highest binding energy) for the natural adenylate (or AMO with carbon atoms in medium blue), aspartol-AMP (or AOA, in green) and Asp-AMS (or AMS, in yellow). The protein backbone (with the antiparallel β-sheet characteristic of class II aaRSs) is represented in blue. Small variations are observed at the connection of the two adenylate moieties, whereas the position of the aspartate side chains and of the adenine ring is almost conserved. (B) Average docking scores obtained for the three substrates (same color code) in the active site of five AspRSs. Scores are indicated in theoretical pK_i values based on computed binding energies (see Materials and methods). (For interpretation of color in this figure, the reader is referred to the web version of this article.)

crystallographic structures of human mt-AspRS in its *apo* and liganded versions, as well as of the other AspRSs investigated in this work, except the *E. coli* enzyme [26], a structural analysis of AspRSs completed by docking studies of the adenylates in the active site of AspRSs can be useful.

AspRSs are modular proteins that belong to class IIb aaRSs. Their catalytic core encompasses a seven-stranded antiparallel β-sheet, surrounded by α-helices that encompass the three class II signature motifs. This fold is common to all class II aaRSs and differs from the Rossmann-fold of class I aaRSs [41,42]. The β-sheet offers a platform where adenylates are formed. The overall structure and the catalytic core of AspRSs are roughly conserved in evolution, but present idiosyncrasies specific to phylogenic kingdoms (lower and higher eukarya, bacteria, archaea and organelles) (reviewed in Ref. [43]).

Interestingly, crystallographic structures tell us that the interaction of aspartyl-adenylate with AspRSs is essentially the same than with free aspartate and the adenosine moiety of ATP. Indeed, as found with *E. coli* AspRS (Fig. 7), the AMP moiety of aspartyl-adenylate is positioned in a class II conserved manner, with interactions of the α-phosphate with conserved Arg217 (Arg266 in mt-AspRS) from motif 2. Further, recognition of the α-carboxyl and α-amino groups of aspartate by conserved AspRS residues is also class II characteristic, but with a system-specific interaction of the side chain carboxylic group with Lys198, Arg489 (Lys247 and Arg542 in mt-AspRS) whose basic side chains are stabilized by salt bridges with Asp233, Glu235 (would be Asp282 and Glu284 in mt-AspRS). Comparison between the *E. coli* AspRS structure containing aspartyl-adenylate and the *apo* structure shows that there is no conformational change whatsoever of the four conserved residues Lys198, Asp233, Glu235 and Arg489 (correspond to Lys247, Asp282, Glu284, Arg542 in mt-AspRS) from the catalytic domain upon aspartate binding [26]. This implies a "lock-and-key" recognition of the preformed adenylate analogs that is also found in archaeal AspRS from *Pyrococcus kodakaraensis* [44] and contrasts with the induced fit occurring upon recognition of ATP with conformational changes in the active site of the *E. coli* enzyme, in particular at Arg217.

On the other hand, sequence analysis of human mt-AspRS [2], together with modeling of its three-dimensional structure (based on the structure of *E. coli* AspRS:tRNA^{Asp}:adenylate ternary complex, see Materials and methods) and docking of the adenylates, indicates similar interaction patterns of the adenylates (see Fig. 5). The amino acids in human mt-AspRS and *E. coli* AspRS identified by the docking procedure to make energetically favorable bonds with the adenylates or to be in vicinity of the adenylate in the active cavity of the AspRSs are shown in Fig. 7. Among these 24 amino acids, 10 were identified by crystallography to play a role in catalysis (see legend to Fig. 7) and only 3 differ in the two enzymes, namely Ile536, Ile581 and Leu583 in mt-AspRS, replaced respectively by Phe533, Val483 and Leu531 in *E. coli* AspRS. These amino acids are not predicted to make energetically favorable bounds with the adenylate, and in addition were not identified by crystallography to contribute to adenylate binding in *E. coli* AspRS. This suggests that the functional differences between the two AspRSs are due to subtle structural effects and are not accounted by sole thermodynamic binding features but are also kinetically driven with induced fit and indirect effects. Such an interpretation finds support from a mutational analysis of the active site of yeast AspRS that identified 23 functionally important amino acids by a genetic selection method. Among these amino acids located around the ATP binding site, 10 act indirectly and were not identifiable by crystallography [45].

In conclusion this analysis suggests that the K_m and K_i variations observed in the test tube are not only the consequence of the architecture of the active site itself and of the direct atomic environment of the ligands, but also rely on the dynamics of ligand binding, tRNA and small substrates, and the associated conformational changes. In this process, adaptability of the flexible tRNA molecule on the protein will likely be crucial [46]. Deciphering these subtleties of human mt-AspRS will require more functional and structural work. In regard to functional investigation, it should

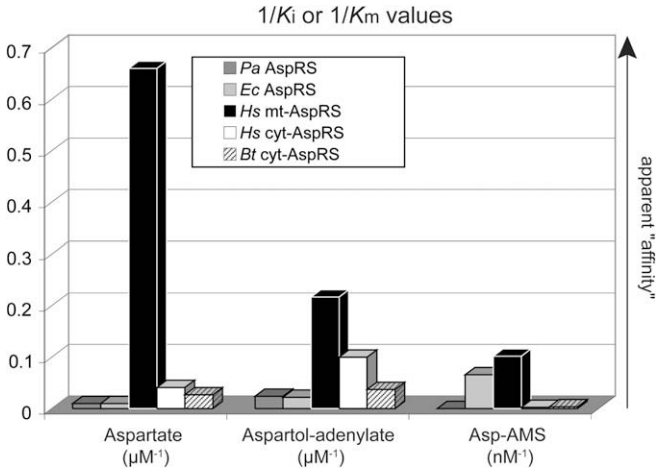

Fig. 6. Histogram comparing the ($1/K_m$) values of aspartate and the ($1/K_i$) values of the two non-hydrolysable aminoalcohol (aspartol-AMP) and sulfamoyl (Asp-AMS) derivatives for five different AspRSs. Abbreviations used: *Pa*, *Pseudomonas aeruginosa*; *Ec*, *Escherichia coli*; *Hs*, *Homo sapiens*; *Bt*, *Bos taurus*. Experimental data for *Pa* and *Ec* AspRSs are taken from Ref. [22].

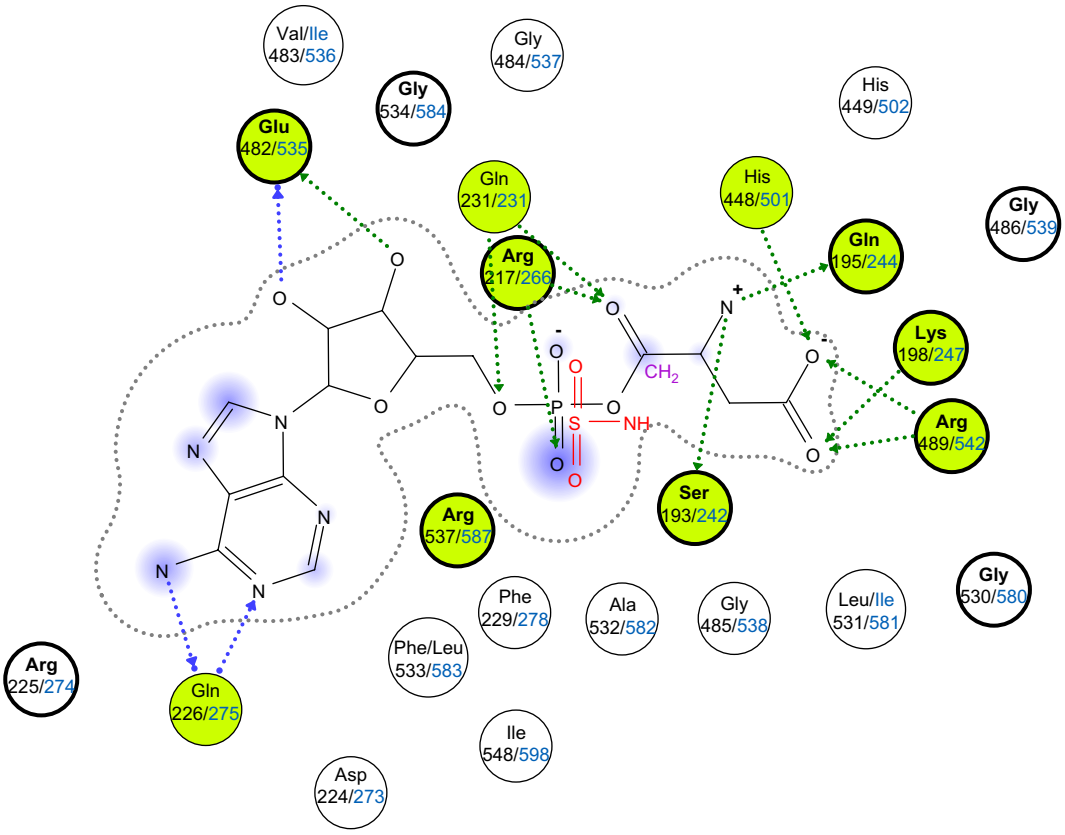

Fig. 7. Schematized comparison of the active sites of *H. sapiens* mt-AspRS and *E. coli* AspRS in interaction with aspartyl-adenylate and its two analogs, Asp-AMS and aspartol-AMP. The figure shows the chemical structure of aspartyl-adenylate and the structural changes in Asp-AMS (in red) and aspartol-AMP (in magenta). The dashed line is the computed proximity contour of the adenylates in the binding cavity of AspRSs. The diameter of the shadowed blue circles is proportional to exposure of adenylate atoms to the solvent. The amino acids forming the catalytic cavity are shown circled in three-letter abbreviations and numbering as in *E. coli* and human mitochondrial AspRSs (colored black and blue, respectively). The 10 amino acids in *E. coli* AspRS that play a role in catalysis [26,43], and present in human mt-AspRS, are displayed on a green background. Notice that Lys198 and Arg489 were also predicted by free energy simulations to be the main contributors for the specificity of aspartate recognition by AspRSs [51]. Conserved residues in all AspRSs are in bold, the other amino acids being semi-conserved and characteristic of bacterial- and mt-AspRSs. The green and blue arrows show respectively the amino acid side chains or backbones predicted by the docking simulations to hydrogen bond with atoms from the adenylates. Note that several putative bonds are not possible with the analogs. (For interpretation of color in this figure, the reader is referred to the web version of this article.)

be kept in mind that the aminoacylation reaction is a two-step process including (i) formation of the aminoacyl-adenylate and (ii) transfer of the amino acid to the tRNA. Accordingly, the K_i value is not necessarily equal to the dissociation constant of the inhibitor for the enzyme/inhibitor complex. Different relative rates of the two steps of the reaction may account at least in part for the difference between the K_i values observed with mt-AspRS and cyt-AspRS. In regard to further structural investigations, we noticed that the strong binding of Asp-AMS, that differentiates the mt-enzyme from other AspRSs, decreases its propensity to aggregate and increases its solubility (not shown). Such a property, also found in the case of human mt-TyrRS [2,47], becomes a positive hint towards successful crystallization assays.

4.5. Outlook

The dramatic adaptation of pathogens to antibiotics calls for new target macromolecules and new types of inhibitors. Along evolution, aaRSs acquired subtle differences in their active site, making this family of macromolecules attractive targets in such a strategy [14–18]. Efficient inhibition by adenylate analogs has already been obtained for bacterial AspRS [22], IleRS [48–50], MetRS [50], GluRS [24] and GlnRS [24]. Our present data confirm and extend a differential sensitivity of AspRSs from various organisms to aspartyl-adenylate analogs. Asp-AMS is the most active inhibitor with K_i values in the nanomolar range, with a stronger effect on bacterial AspRSs (*E. coli* and *P. aeruginosa*) than on human cytosolic AspRS. Here, for the first time, a very strong inhibition by Asp-AMS of a human mitochondrial synthetase has been measured. These data suggest that medical applications of aaRS substrate analogs as inhibitors of pathogens could potentially affect the host mitochondrial enzymes. Since mitochondria are the powerhouse of eukaryal cells, side effects can indeed not be ruled out. However, the toxicity of adenylate analogs *in vivo* is difficult to predict precisely since it will depend also on the ability of the drug to cross the mitochondrial membranes and further on the intra mitochondrial concentration of free amino acid competing with the drug for the active site of the synthetase. Additional investigations need to be performed to understand the contribution of these parameters in detail.

Acknowledgments

M. Frugier is acknowledged for the generous gift of human cyt-AspRS. This work was supported by a collaborative France-Québec grant (project #61.103). We thank also Centre National de la Recherche Scientifique (CNRS) including a PICS project, Université Louis Pasteur Strasbourg (ULP), Association Française contre les Myopathies (AFM) in France and the Fonds Québécois de Recherche sur la Nature et les Technologies (FQRNT) in Canada for financial support. M.M. received a fellowship from the French Ministère de l'Enseignement Supérieur et de la Recherche.

References

[1] I.E. Scheffler, Mitochondria, second ed. Willey-Liss, 2007.
[2] L. Bonnefond, A. Fender, J. Rudinger-Thirion, R. Giegé, C. Florentz, M. Sissler, Towards the full set of human mitochondrial aminoacyl-tRNA synthetases: characterization of AspRS and TyrRS, Biochemistry 44 (2005) 4805–4816.
[3] M. Sissler, B. Lorber, M. Messmer, A. Schaller, J. Pütz, C. Florentz, Handling mammalian mitochondrial tRNAs and aminoacyl-tRNA synthetases for functional and structural characterization, Methods 44 (2008) 176–189.
[4] K. Shiba, P. Schimmel, H. Motegi, T. Noda, Human glycyl-tRNA synthetase. Wide divergence of primary structure from bacterial counterpart and species-specific aminoacylation, J. Biol. Chem. 269 (1994) 30049–30055.
[5] S.J. Mudge, J.H. Williams, H.J. Eyre, G.R. Sutherland, P.J. Cowan, D.A. Power, Complex organisation of the 5′-end of the human glycine tRNA synthetase gene, Gene 209 (1998) 45–50.
[6] E. Tolkunova, H. Park, J. Xia, M.P. King, E. Davidson, The human lysyl-tRNA synthetase gene encodes both the cytoplasmic and mitochondrial enzymes by means of an unusual splicing of the primary transcript, J. Biol. Chem. 275 (2000) 35063–35069.
[7] L. Margulis, Origin of Eukaryotic Cells, New Haven Yale University Press, 1970.
[8] M.W. Gray, G. Burger, B.F. Lang, The origin and early evolution of mitochondria, Genome Biol. 2 (2001) 1018.1–1018.5.
[9] B. Brindefalk, J. Viklund, D. Larsson, M. Thollesson, S.G. Andersson, Origin and evolution of the mitochondrial aminoacyl-tRNA synthetases, Mol. Biol. Evol. 24 (2007) 743–756.
[10] L. Bonnefond, M. Frugier, E. Touzé, B. Lorber, C. Florentz, R. Giegé, C. Sauter, J. Rudinger-Thirion, Crystal structure of human mitochondrial tyrosyl-tRNA synthetase reveals common and idiosyncratic features, Structure 15 (2007) 1505–1516.
[11] A. Fender, C. Sauter, M. Messmer, J. Pütz, R. Giegé, C. Florentz, M. Sissler, Loss of a primordial identity element for a mammalian mitochondrial aminoacylation system, J. Biol. Chem. 281 (2006) 15980–15986.
[12] L. Bonnefond, M. Frugier, R. Giegé, J. Rudinger-Thirion, Human mitochondrial TyrRS disobeys the tyrosine identity rules, RNA 11 (2005) 558–562.
[13] Y. Kumazawa, H. Himeno, K.-I. Miura, K. Watanabe, Unilateral aminoacylation specificity between bovine mitochondria and eubacteria, J. Biochem. 109 (1991) 421–427.
[14] J. Tao, P. Schimmel, Inhibitors of aminoacyl-tRNA synthetases as novel antiinfectives, Exp. Opin. Invest. Drugs 9 (2000) 1767–1775.
[15] R. Chênevert, S. Bernier, J. Lapointe, Inhibitors of aminoacyl-tRNA synthetases as antibiotics and tools for structural and mechanistic studies, in: J. Lapointe, L. Brakier-Gringas (Eds.), Translation Mechanisms, Landes Bioscience, 2003, pp. 416–428.
[16] S. Kim, C. Lee, E.C. Choi, S.Y. Choi, Aminoacyl-tRNA synthetases and their inhibitors as a novel family of antibiotics, Appl. Microbiol. Biotechnol. 61 (2003) 278–288.
[17] J. Pohlmann, H. Brotz-Oesterhelt, New aminoacyl-tRNA synthetase inhibitors as antibacterial agents, Curr. Drug Targets Infect. Disord. 4 (2004) 261–272.
[18] M. Torchala, M. Hoffmann, IA, Database of known ligands of aminoacyl-tRNA synthetases, J. Comput. Aided Mol. Des. 21 (2007) 523–525.
[19] A. Fuller, Pseudomonic acid: an antibiotic produced by *Pseudomonas fluorescens*, Nature 234 (1971) 416–417.
[20] J. Hughes, G. Mellows, Inhibition of isoleucyl-transfer ribonucleic acid synthetase in *Escherichia coli* by pseudomonic acid, Biochem. J. 176 (1978) 305–318.
[21] R.O. Nicholas, V. Berry, P.A. Hunter, J.A. Kelly, The antifungal activity of mupirocin, J. Antimicrob. Chemother. 43 (1999) 579–582.
[22] S. Bernier, P.M. Akochy, J. Lapointe, R. Chênevert, Synthesis and aminoacyl-tRNA synthetase inhibitory activity of aspartyl adenylate analogs, Bioorg. Med. Chem. 13 (2005) 69–75.
[23] J. Lapointe, S. Levasseur, D. Kern, Glutamyl-tRNA synthetase from *Escherichia coli*, Methods Enzymol. 113 (1985) 42–49.
[24] C. Balg, S.P. Blais, S. Bernier, J.L. Huot, M. Couture, J. Lapointe, R. Chênevert, Synthesis of beta-ketophosphonate analogs of glutamyl and glutaminyl adenylate, and selective inhibition of the corresponding bacterial aminoacyl-tRNA synthetases, Bioorg. Med. Chem. 15 (2007) 295–304.
[25] M. Ruff, S. Krishnaswamy, M. Boeglin, A. Poterszman, A. Mitschler, A. Podjarny, B. Rees, J.-C. Thierry, D. Moras, Class II aminoacyl transfer RNA synthetases: crystal structure of yeast aspartyl-tRNA synthetase complexed with $tRNA^{Asp}$, Science 252 (1991) 1682–1689.
[26] S. Eiler, A.C. Dock-Bregeon, L. Moulinier, J.-C. Thierry, D. Moras, Synthesis of aspartyl-$tRNA^{Asp}$ in *Escherichia coli* – a snapshot of the second step, EMBO J. 18 (1999) 6532–6541.
[27] A. Sali, T.L. Blundell, Comparative protein modelling by satisfaction of spatial restraints, J. Mol. Biol. 234 (1993) 779–815.
[28] K. Arnold, L. Bordoli, J. Kopp, T. Schwede, The SWISS-MODEL workspace: a web-based environment for protein structure homology modelling, Bioinformatics 22 (2006) 195–201.
[29] R.J. Rosenfeld, D.S. Goodsell, R.A. Musah, G.M. Morris, D.B. Goodin, A.J. Olson, Automated docking of ligands to an artificial active site: augmenting crystallographic analysis with computer modeling, J. Comput. Aided Mol. Des. 17 (2003) 525–536.
[30] P. Berg, E.J. Offengand, An enzymatic mechanism for linking amino acids to RNA, Proc. Nat. Acad. Sci. U.S.A. 44 (1958) 78–86.
[31] J. Lapointe, R. Giegé, Transfer RNAs and aminoacyl-tRNA synthetases, in: H. Trachsel (Ed.), Translation in Eukaryotes, CRC Presss Inc, Boca Raton, FL, 1991, pp. 35–69.
[32] R. Giegé, The early history of tRNA recognition by aminoacyl-tRNA synthetases, J. Biosci. 31 (2006) 477–488.
[33] M. Ibba, D. Söll, Aminoacyl-tRNA synthesis, Annu. Rev. Biochem. 69 (2000) 617–650.
[34] M. Ibba, C. Francklyn, S. Cusack (Eds.), The Aminoacyl-tRNA Synthetases, Landes Bioscience, 2005.
[35] K.B. Jacobson, Reaction of aminoacyl-tRNA synthetases with heterologous tRNA's, Prog. Nucl. Acid Res. Mol. Biol. 11 (1971) 461–488.
[36] A.R. Fersht, J.P. Shi, J. Knill-Jones, D.M. Lowe, A.J. Wilkinson, D.M. Blow, P. Brick, P. Carter, M.M. Waye, G. Winter, Hydrogen bonding and biological specificity analysed by protein engineering, Nature 314 (1985) 235–238.
[37] J. Pütz, J.D. Puglisi, C. Florentz, R. Giegé, Additive, cooperative and anticooperative effects between identity nucleotides of a tRNA, EMBO J. 12 (1993) 2949–2957.
[38] B. Lorber, D. Kern, R. Giegé, J.-P. Ebel, Covalent attachment of aspartic acid to yeast aspartyl-tRNA synthetase, FEBS Lett. 146 (1982) 59–64.
[39] D. Kern, B. Lorber, Y. Boulanger, R. Giegé, A peculiar property of aspartyl-tRNA synthetase from bakers yeast: chemical modification of the protein by the enzymatically synthesized aminoacyl adenylate, Biochemistry 24 (1985) 1321–1332.
[40] D. Bernard, P.M. Akochy, S. Bernier, O. Fisette, O.C. Brousseau, R. Chênevert, P.H. Roy, J. Lapointe, Inhibition by L-aspartol adenylate of a nondiscriminating aspartyl-tRNA synthetase reveals differences between the interactions of its active site with tRNA(Asp) and tRNA(Asn), J. Enzyme Inhib. Med. Chem. 22 (2007) 77–82.
[41] S. Cusack, C. Berthet-Colominas, M. Hartlein, N. Nassar, R. Leberman, A second class of synthetase structure revealed by X-ray analysis of *Escherichia coli* seryl-tRNA synthetase at 2.5 Å, Nature 347 (1990) 249–255.
[42] G. Eriani, M. Delarue, O. Poch, J. Gangloff, D. Moras, Partition of tRNA synthetases into two classes based on mutually exclusive sets of sequence motifs, Nature 347 (1990) 203–206.
[43] R. Giegé, B. Rees, Aspartyl-tRNA synthetases, in: M. Ibba, C. Francklyn, S. Cusack (Eds.), Aminoacyl-tRNA synthetases, Landes Biosciences, 2005, pp. 210–226.
[44] E. Schmitt, L. Moulinier, S. Fujiwara, T. Imanaka, J.-C. Thierry, D. Moras, Crystal structure of aspartyl-tRNA synthetase from *Pyrococcus kodakaraensis* KOD: archeon specificity and catalytic mechanism of adenylate formation, EMBO J. 17 (1998) 5227–5237.
[45] L. Ador, A. Camasses, P. Erbs, J. Cavarelli, D. Moras, J. Gangloff, G. Eriani, Active site mapping of yeast aspartyl-tRNA synthetase by *in vivo* selection of enzyme mutations lethal for cell growth, J. Mol. Biol. 288 (1999) 231–242.
[46] R. Giegé, Toward a more complete view of tRNA biology, Nat. Struct. Mol. Biol. 15 (2008) 1007–1014.
[47] M. Sissler, J. Pütz, F. Fasiolo, C. Florentz, Mitochondrial aminoacyl-tRNA synthetases, in: M. Ibba, C. Francklyn, S. Cusack (Eds.), Aminoacyl-tRNA synthetases, Landes Biosciences, 2005, pp. 271–284.
[48] A.J. Pope, M. McVey, K. Fantom, K.J. Moore, Effects of substrate and inhibitor binding on proteolysis of isoleucyl-tRNA synthetase from *Staphylococcus aureus*, J. Biol. Chem. 273 (1998) 31702–31706.
[49] C.F. Crasto, A.K. Forrest, T. Karoli, D.R. March, L. Mensah, P.J. O'Hanlon, M.R. Nairn, M.D. Oldham, W. Yue, M.G. Banwell, C.J. Easton, Synthesis and activity of analogues of the isoleucyl tRNA synthetase inhibitor SB-203207, Bioorg. Med. Chem. 11 (2003) 2687–2694.
[50] J. Lee, S.E. Kim, J.Y. Lee, S.Y. Kim, S.U. Kang, S.H. Seo, M.W. Chun, T. Kang, S.Y. Choi, H.O. Kim, N-Alkoxysulfamide, N-hydroxysulfamide, and sulfamate analogues of methionyl and isoleucyl adenylates as inhibitors of methionyl-tRNA and isoleucyl-tRNA synthetases, Bioorg. Med. Chem. Lett. 13 (2003) 1087–1092.
[51] G. Archontis, T. Simonson, D. Moras, M. Karplus, Specific amino acid recognition by aspartyl-tRNA synthetase studied by free energy simulations, J. Mol. Biol. 275 (1998) 823–846.